Cell Reports
Article

Gli3 Repressor Controls Cell Fates and Cell Adhesion for Proper Establishment of Neurogenic Niche

Hui Wang,[1,3] Anna W. Kane,[1,2,3] Cheol Lee,[1] and Sohyun Ahn[1,*]
[1]Program in Genomics of Differentiation, Eunice Kennedy Shriver National Institute of Child Health and Human Development, National Institutes of Health, Bethesda, MD 20892, USA
[2]Brown-NIH Graduate Partnership Program, Department of Neuroscience, Brown University, Providence, RI 02912, USA
[3]Co-first author
*Correspondence: ahnsohyun@mail.nih.gov
http://dx.doi.org/10.1016/j.celrep.2014.07.006

SUMMARY

Neural stem cells (NSCs) in the subventricular zone (SVZ) rely on environmental signals provided by the neurogenic niche for their proper function. However, little is known about the initial steps of niche establishment, as embryonic radial glia transition to postnatal NSCs. Here, we identify Gli3 repressor (Gli3R), a component of the Sonic hedgehog (Shh) pathway, as a critical factor controlling both cell-type specification and structural organization of the developing SVZ. We demonstrate that Gli3R expressed in radial glia temporally regulates gp130/STAT3 signaling at the transcriptional level to suppress glial characteristics in differentiating ependymal cells. In addition, Gli3R maintains the proper level of Numb in ependymal cells to allow localization of cell adhesion molecules such as vascular cell adhesion molecule (VCAM) and E-cadherin. Thus, our findings reveal a role for Gli3R as a mediator of niche establishment and provide insights into the conditions required for proper SVZ neurogenic niche formation.

INTRODUCTION

Neurogenesis persists in the subventricular zone (SVZ) of the lateral ventricle in the postnatal rodent forebrain (Kriegstein and Alvarez-Buylla, 2009). In the SVZ, neural stem cells (NSCs) are in close contact with ependymal cells, transit-amplifying cells, neuroblasts, and endothelial cells (Doetsch et al., 1997). Collectively, these cells constitute the neurogenic niche. The ventricular surface of the SVZ is covered with ependymal cells that surround NSCs in pinwheel-like arrangements (Mirzadeh et al., 2008). These stereotypical arrangements of distinct cell types in the SVZ appear important for providing NSCs with the necessary environmental signals for proper production of interneurons of the olfactory bulb (Ihrie and Alvarez-Buylla, 2011; Tavazoie et al., 2008; Shen et al., 2008).

The neurogenic SVZ in postnatal animals is derived from the embryonic ventricular zone (VZ) of the lateral ganglionic eminence (LGE) (Young et al., 2007). Around birth, radial glial cells (RGCs) in the VZ of the LGE transform into postnatal NSCs and ependymal cells (Kriegstein and Alvarez-Buylla, 2009). Very little is known about how adult NSCs form from embryonic radial glia, and understanding the differential signaling events directing NSC and ependymal cell formation would give us an idea of how adult NSCs are initially established and regulated.

One critical environmental signal, Sonic hedgehog (Shh), has been known to control the maintenance and proliferation of NSCs (Machold et al., 2003; Ahn and Joyner, 2005) and other neural progenitors (Corrales et al., 2006) in adults. Interestingly, Shh-responding NSCs do not emerge until late embryonic stages in the SVZ and are not fully directing neurogenesis until after birth (Ahn and Joyner, 2005). However, prior to Shh signaling activation, the RGCs in the VZ do express downstream components of the pathway, including *Gli2* (Allen Brain Atlas; http://developingmouse.brain-map.org) and *Gli3* (Wang et al., 2011). It is well known that *Gli3*, in particular, plays a critical role as a repressor (Gli3 repressor [Gli3R]) in brain patterning in embryonic development in the absence of Shh signaling (Theil et al., 1999). The presence of Shh effectors in the absence of active Shh signaling raises the question as to whether Gli3 in the VZ (the future SVZ) plays any role prior to Shh signaling activation in the neurogenic niche development.

Shh signaling is not the only signaling pathway critical for formation of the neurogenic niche. Postnatal SVZ NSCs inherit glial cell features from RGCs and turn on GFAP expression around birth as well (Kriegstein and Alvarez-Buylla, 2009). gp130/JAK-STAT signaling promotes glial fate and activates the *GFAP* promoter during normal gliogenesis (Bonni et al., 1997; Nakashima et al., 1999a, 1999b; Takizawa et al., 2001). gp130/JAK-STAT signaling is shared by the interleukin-6 (IL-6) family cytokines, including CNTF, OSM, IL-6, LIF, and CT-1 (Nakashima and Taga, 2002). Although CNTF is the major in vivo glial fate promoting cytokine during development, all five signals have the ability to induce GFAP+ glial cells in vitro due to the common downstream signal pathway involving activation of the STAT family transcription factors (Nakashima and Taga, 2002). However,

how STAT signaling is specifically activated in postnatal NSCs and how it interacts with Shh signaling remain unclear.

Not all RGCs become postnatal NSCs, however. They also form ependymal cells (Spassky et al., 2005), another important cell population in homeostasis of postnatal neurogenesis in the SVZ. Instead of taking on glial characteristics, these cells differentiate into cuboid, multiciliated cells that are required for circulating cerebrospinal fluid (CSF) (Spassky et al., 2005). Very little is understood about the nature of the signals that instruct ependymal development, but it has been shown that Numb and Numblike are required for the formation and maintenance of ependymal cells in the SVZ (Kuo et al., 2006). Numb is a well-known negative regulator of the Notch signaling pathway that degrades Notch intracellular domain (Di Marcotullio et al., 2011). In addition, Numb also plays a role in maintaining RGC polarity and apical adhesion during development in the SVZ as an endocytic adaptor (Rasin et al., 2007; Zhou et al., 2011). These apical adhesions between NSCs and ependymal cells are required for proper NSC function (Karpowicz et al., 2009; Paez-Gonzalez et al., 2011). For example, disruption of several cell adhesion molecules including Ankyrin-3, vascular cell adhesion molecule-1 (VCAM1), and E-cadherin has been shown to impair the SVZ structure and NSC function (Paez-Gonzalez et al., 2011; Kokovay et al., 2012; Karpowicz et al., 2009). Furthermore, E-cadherin localization is also regulated through Numb (Rasin et al., 2007), emphasizing the importance of Numb in the neurogenic SVZ.

Although the Shh, Notch, and gp130/STAT signaling pathways all have been implicated in the maintenance of the adult neurogenic niche, less is known about the way in which the niche is originally formed. Because previous work in our lab identified the importance of Gli3R, the repressor of the Shh pathway, in specifying neural progenitor fates (Wang et al., 2011), we asked whether Gli3R plays a role in fate specification of NSCs in the SVZ. We also probed whether Gli3R interacts with other pathways to establish as well as maintain the neurogenic niche. We found that Gli3 acts as a repressor in the developing neurogenic niche to promote fate specification of both NSCs and ependymal cells and in establishment of the SVZ niche structure.

RESULTS

The Establishment of Postnatal NSC Niche Is Disrupted in the Absence of *Gli3*

Gli3, which serves as a context-dependent regulator of the Shh pathway, is expressed in the VZ/SVZ of the brain, including the developing LGE (Schimmang et al., 1992; Fotaki et al., 2006; Wang et al., 2011). *Gli3* expression was also detected in both NSCs and ependymal cells of the SVZ in the adult brain (Figure S1C) (Lee et al., 2012). In contrast, Shh-positive signaling as measured by *Gli1* expression (Bai et al., 2002) is only expressed in a very limited fashion embryonically and is not required for olfactory bulb neurogenesis until embryonic day 18.5 (E18.5) (Ahn and Joyner, 2005). In adults, Shh signaling activation was only detected in cells capable of proliferation (NSCs and transit-amplifying cells) in the postnatal SVZ (Ahn and Joyner, 2005; Figure S1B). Together, the expression data suggest that Gli3 protein likely functions as a repressor (Gli3R) in RGCs during development and in postnatal ependymal cells (Figure S1A).

We investigated the earlier role of *Gli3* (as Gli3R) by conditionally removing it in RGCs with *Nestin-Cre* (*NC*) mice (Tronche et al., 1999) before active Shh signaling emerges in the ventral SVZ (Ahn and Joyner, 2005), but after the embryonic patterning is established (Wang et al., 2011). We first analyzed the structure of the developing neurogenic niche on the lateral wall of the lateral ventricles (Figure 1A). Whole-mount analysis of the SVZ showed a pinwheel-like arrangement of NSCs (GFAP+) and ependymal cells (β-catenin+ for cellular morphology and γ-tubulin+ for basal bodies of cilia) (Mirzadeh et al., 2008) in the control brain by postnatal day 7 (P7) (Figure 1B). NSCs were located in the center of intercellular spaces between ependymal cells (Figures 1B and 1D). In contrast, the *NC;Gli3*^{cko} mutants did not show any apparent pinwheel-like structure (Figures 1C and 1E). Expression of the NSC marker, GFAP, was generally upregulated in RGC-like cells as identified by a single prominent basal body in *NC;Gli3*^{cko} mutants (Figure 1C, arrows). These RGC-like cells are only found in the mutant samples, suggesting a delay in niche maturation in *NC;Gli3*^{cko} mutants (Figure S1D). At P21, GFAP expression persisted in mutant cells exhibiting numerous γ-tubulin+ ciliary basal bodies, a hallmark of mature ependymal cells (Figure 1E). This ectopic GFAP expression indicates that a clear distinction between NSCs and ependymal cells fails to develop when *Gli3* is absent.

In order to confirm the lack of proper cell fate specification in our *NC;Gli3*^{cko} mutants, we performed immunohistochemical staining for FoxJ1, a marker for mature ependymal cells (Jacquet et al., 2009). We found that fewer FoxJ1+ cells were present in the *NC;Gli3*^{cko} mutant SVZ at P4 (Figure S1F), compared to control (Figure S1E; quantified in Figure S1G). By P7, the *NC;Gli3*^{cko} mutant SVZ expressed FoxJ1 at equivalent levels to the control, but the majority of FoxJ1+ cells coexpressed GFAP (Figure 1I), whereas the control showed rarely any FoxJ1+ GFAP+ cells (Figure 1H). Quantification revealed a 6-fold increase in the amount of FoxJ1+ GFAP+ cells in the *NC;Gli3*^{cko} mutant SVZ (Figure 1J). Together, these results indicate that there is a delay in ependymal maturation followed by confusion of cell fate specification that leads to the malformation of the neurogenic niche observed at P21 (Figure 1E).

Because the ability to respond to Shh signaling is one major distinction between NSCs (Ahn and Joyner, 2005) and ependymal cells in the SVZ (Figure S1B), we examined Shh responsiveness in the *NC;Gli3*^{cko} mutant SVZ. The *Gli1*^{nLZ} allele allowed us to visualize the cells responding to Shh signaling based on X-gal precipitates identified by transmission electron microscopy (TEM) analysis. In controls, there was a clear distinction between cells that respond to Shh signaling with strong X-gal precipitates (NSCs) and cells that do not respond (ependymal cells) (Figure S1H). In contrast, it was hard to distinguish the cells with a clear strong presence of X-gal precipitates in the *NC;Gli3*^{cko} mutant SVZ (Figure S1H). Blind scoring for the strength of Shh responsiveness showed that instead of clear separation between NSCs and ependymal cells, most of the cells in the *NC;Gli3*^{cko} mutant SVZ exhibited intermediate Shh responsiveness (Figure S1I). The lack of differential Shh activation between NSCs and ependymal cells is another indication that these

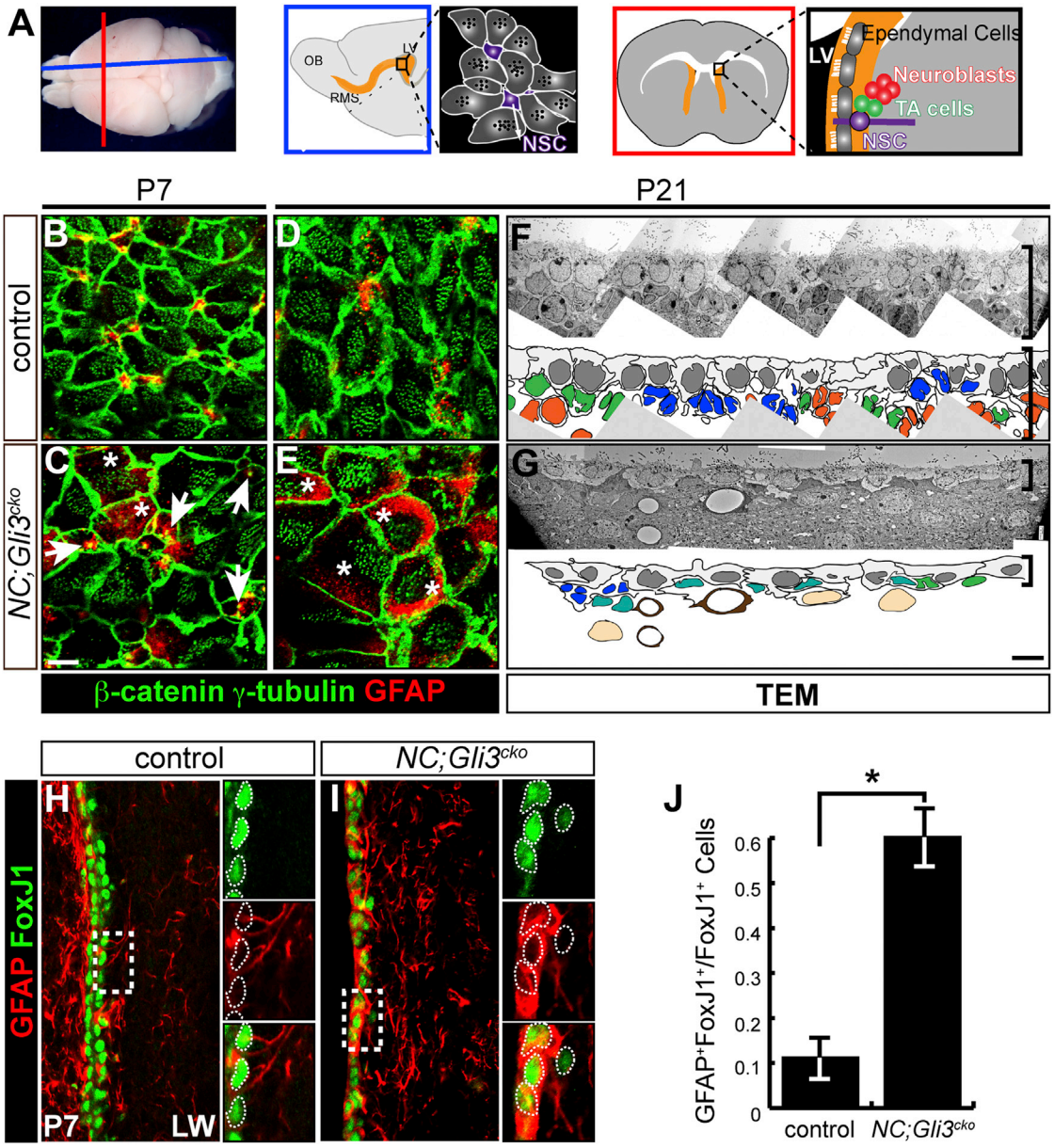

Figure 1. *Gli3* Is Required for Proper Establishment of the Neurogenic Niche in the SVZ

(A) Schematics of mouse brain cut along the sagittal (blue) and coronal (red) orientation show the arrangement of cell types found in the neurogenic SVZ, including NSCs, transit-amplifying (TA) cells, ependymal cells, and neuroblasts. LV, lateral ventricle; OB, olfactory bulb; RMS, rostral migratory stream.

(B–E) En face view of the lateral wall of the ventricle shows that the pinwheel-like arrangements of ependymal cells (β-catenin+, green cell border; γ-tubulin+, green dots) and NSCs (GFAP+, red) are established by P7 in the controls (B and D). *NC;Gli3*^{cko} mutants that lack Gli3 function in embryonic RGCs show persistence of RGCs with a single basal body (white arrows) and no clear pinwheel arrangements and ectopic expression of GFAP within β-catenin+ γ-tubulin+ cells (C and E, white asterisks). Scale bar, 5 μm.

(F and G) TEM analysis of the control (F) and *NC;Gli3*^{cko} mutants (G). Disrupted cytoarchitecture of the SVZ is shown in the mutants. The SVZ cell types are indicated in colors: blue (NSC), green (TA cell), orange (neuroblast), gray (ependymal cell), teal (atypical cells), and light brown (striatal neurons). Brackets indicate the thickness of the SVZ. Scale bar, 5 μm.

(H–J) Immunohistochemistry of FoxJ1 (green) and GFAP (red) staining in control (H) and *NC;Gli3*^{cko} (I) SVZ at P7. FoxJ1 expression is similar between control and *NC;Gli3*^{cko} SVZ, but many more cells coexpress GFAP and FoxJ1 in the *NC;Gli3*^{cko} mutant (I) as compared to the control (H, quantified in J). Insets reveal colocalization of FoxJ1 and GFAP, with white dashed lines encircling FoxJ1+ cells. Scale bar, 10 μm. Error bars represent SEM. *$p < 0.05$.

See also Figure S1.

mutant cells are not establishing proper cell identities during niche maturation.

We further confirmed an abnormal SVZ cytoarchitecture in *NC;Gli3*^{cko} mutants at the ultrastructural level using TEM. Based on the identification criteria of the SVZ cell types described in Doetsch et al. (1997), we were able to assign cell identities in the control SVZ (Figure 1F). However, in the *NC;Gli3*^{cko} mutants, there were numerous cells without clear characteristic features of NSCs, transit-amplifying cells, or neuroblasts (Figure 1G). The outermost layer of the SVZ containing ependymal cells was morphologically atypical and did not intercalate extensively in *NC;Gli3*^{cko} mutants (Figure 1G). In addition, the *NC;Gli3*^{cko} SVZ was much thinner than the control SVZ (brackets in Figures 1F and 1G), indicating severe structural defects caused by a loss of *Gli3* during development.

As a result of this improper fate specification, these *Gli3* mutant cells with dual cellular characteristics do not function properly as NSCs or ependymal cells. They are not proliferative (Figure S3D) and, thus, do not function as NSCs. They also do not circulate CSF, as evidenced by the severe hydrocephalus in *NC;Gli3*^{cko} mutant mice (unpublished data).

Although we thought it likely that *Gli3* itself was responsible for niche maturation, we wanted to ensure that the derepression of the Shh pathway induced by loss of *Gli3* was not responsible for our observed findings. In order to assess ectopic Shh activation, we crossed our *NC;Gli3*^{cko} mice with *Gli1*^{nLZ}, a reporter that expresses LacZ in any cell responsive to Shh signaling. X-gal staining for LacZ revealed no overall increase in *Gli1* expression in the *NC;Gli3*^{cko} SVZ as compared to the control (Figure S1J), suggesting that activation of Shh signaling is not increased in the absence of *Gli3*.

In order to confirm that Shh activation was not playing a role in maturation of the adult neurogenic niche, we ablated Shh-positive signaling directly. First, we ablated *Smoothened* (*Smo*), one of the main transducers of Shh activation, via *NC*. We found that loss of *Smo* did not result in mixed identity cells or disorganization of niche structure in the SVZ (Figure S1K). We also used *NC* to ablate *Gli2*, the major transcriptional activator of the Shh pathway. In the absence of *Gli2*, there was no difference in the cytoarchitecture and cell identity between the control and *NC;Gli2*^{cko} mutant SVZ (Figure S1L). Together, these experiments indicate that niche structure and cell fate are not governed by activation of Shh signaling but, rather, the presence of Gli3R.

Loss of Gli3R Leads to Overexpression of gp130

In order to find the downstream events leading to the ectopic expression of GFAP in *Gli3* mutant SVZ, we carried out a quantitative real-time PCR-based gene expression analysis for genes that are involved in Shh and/or Notch pathways (QIAGEN RT^2 Profiler PCR Array) and were previously identified to contain Gli3 binding sites (Vokes et al., 2008). We compared E16.5 forebrain tissue from wild-type (WT) embryos with that from *Gli3*$^{Xt/Xt}$ null mutant animals to observe the maximum difference in gene expression caused by the absence of *Gli3*. Because active Shh signaling is absent in E16.5 forebrain (data not shown), any phenotypes observed in *Gli3*$^{Xt/Xt}$ null mutants could be attributed to the loss of Gli3R. Surprisingly, one of the dramatically changed genes was *il6st*, which encodes a protein named gp130. gp130 is a coreceptor subunit shared by the IL-6 family of cytokines including CNTF, OSM, IL-6, LIF, and CT-1 (Nakashima and Taga, 2002). gp130 and the cytokine-specific receptors transduce cytokine signals and activate downstream effectors, including JAK-STAT molecules. In E16.5 forebrain, the mRNA of *il6st* was increased by 5.75 ± 0.24-fold in *Gli3*$^{Xt/Xt}$ null mutants compared to WT controls (Figure 2A). However, the expression levels of all the cytokine-specific coreceptors were unchanged (Figure 2A). Consistent with the mRNA expression level, gp130 protein level was increased by 3.64 ± 0.07-fold in E16.5 mutant forebrain compared to the WT (Figures 2B and 2C). Based on the *Gli3* null mutant embryo results, we next asked whether similar molecular changes occurred in *NC;Gli3*^{cko} mutants. RNA in situ hybridization revealed that *il6st* expression was clearly increased in the postnatal SVZ in the *NC;Gli3*^{cko} mutants (Figure 2D).

We then tested whether the ectopic upregulation of *il6st* was due to the loss of Gli3R, which normally acts as a transcriptional repressor. We identified two putative Gli binding sites sharing the same consensus core sequence between −215 and −200 bp upstream of the *il6st* transcription initiation site in the mouse genome (Evolutionary Conserved Regions Browser [Ovcharenko et al., 2004] and rVISTA [Loots and Ovcharenko, 2004]). Electrophoretic mobility shift assay (EMSA) confirmed the direct and specific binding of Gli3R to the identified Gli sites taken from the *il6st* gene (Figure 2E).

Previous studies indicated that all IL-6 family cytokines have the ability to induce GFAP+ glial cell fate in vitro due to common downstream activation of JAK-STAT3 signaling (Nakashima and Taga, 2002). Thus, we examined the changes in cytokine levels in the *Gli3* null mutants using quantitative real-time PCR. Interestingly, at E16.5, *OSM* and *IL-6* were both expressed at significantly higher levels in *Gli3*$^{Xt/Xt}$ mutants compared to controls (4.03 ± 0.24-fold and 2.77 ± 0.24-fold, respectively) (Figure S2A). We found that *OSM* mRNA expression was also upregulated in the postnatal SVZ of *NC;Gli3*^{cko} mutants as expected (Figure S2B). Together, our results indicate that the absence of Gli3R causes overexpression of both ligands and a shared receptor subunit of the IL-6 cytokine family.

Loss of Gli3R Induces the Sustained Activation of STAT3 and Overexpression of GFAP in *Gli3* Mutant SVZ

gp130 promotes GFAP expression and glial cell fate through the phosphorylation of the STAT3 (pSTAT3) transcription factor (Nakashima et al., 1999a, 1999b; Bonni et al., 1997). In control animals, there was a transient activation of STAT3 in a small population of SVZ cells at P4 (Figure S3A), but pSTAT3 was barely detectible by P7 (Figure 3A) (Herrmann et al., 2008). In contrast, *NC;Gli3*^{cko} mutants showed widespread presence of pSTAT3 in the SVZ at both P4 and P7 (Figures S3B and 3B). In addition, most of the pSTAT3+ cells also expressed GFAP, indicating that the increased gp130 level induced ectopic activation of STAT3 to induce GFAP overexpression in *NC;Gli3*^{cko} mutants.

To further confirm that the sustained activation of STAT3 and overexpression of GFAP in *NC;Gli3*^{cko} mutants were solely dependent on the loss of *Gli3*, we acutely induced *Gli3* mutant

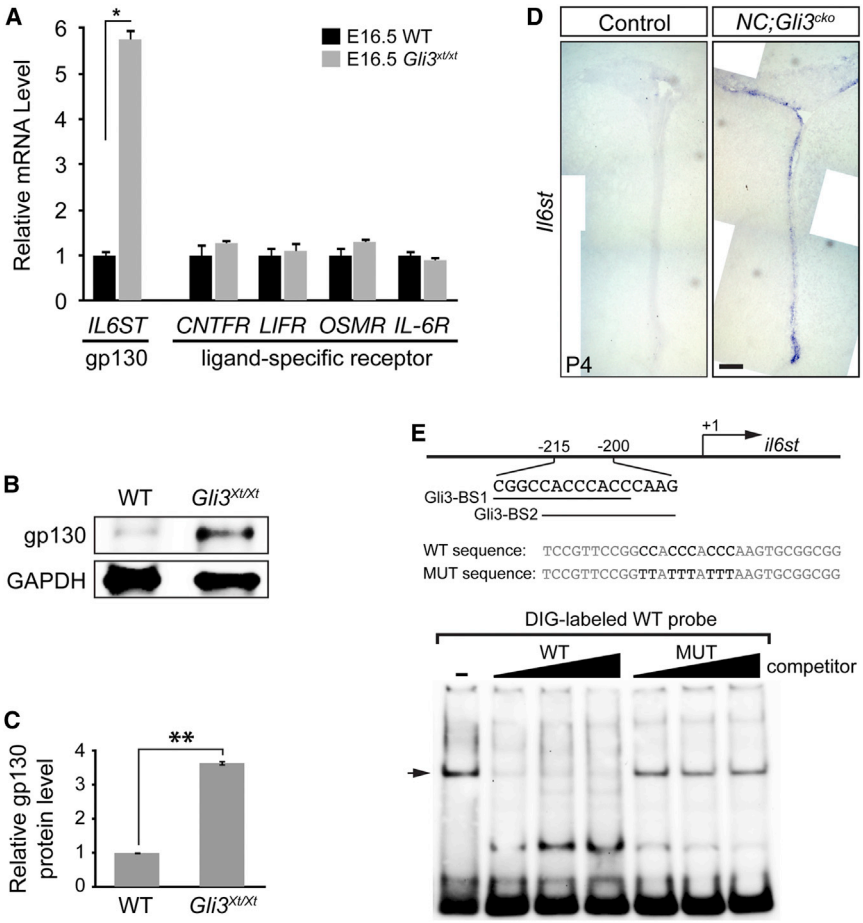

Figure 2. *Il6st* Transcription Is Repressed by Gli3R

(A) Quantitative real-time PCR shows that *Il6st* (gp130) mRNA is increased in E16.5 forebrain of $Gli3^{Xt/Xt}$ compared to WT. mRNA level of the IL-6 cytokine family ligand-specific receptors is not different between WT and $Gli3^{Xt/Xt}$ at E16.5. Error bars represent SEM. *p = 0.016.

(B and C) Western blot shows that gp130 protein is increased in E16.5 forebrain of $Gli3^{Xt/Xt}$ compared to WT. Error bars indicate SEM. **p < 0.001.

(D) In situ hybridization on control and $NC;Gli3^{cko}$ shows that *Il6st* mRNA is increased in the mutant SVZ at P4. Scale bar, 500 μm.

(E) EMSA shows that Gli3R binds to two overlapping putative Gli binding sites located between −215 and −200 bp 5′ of mouse *il6st* gene. +1 indicates the transcription initiation site of the *il6st* gene. The arrow indicates the complex of Gli3R and DIG-labeled WT probe. MUT, mutant.

See also Figure S2.

cells in a WT environment by electroporating *Cre*-expressing plasmids into $Gli3^{F/F}$ embryos at E13.5 (Figure 3G). We found that by P7, Cre-expressing *Gli3* mutant cells in the SVZ showed ectopic activation of STAT3 (Figure 3I) and overexpression of GFAP (Figure 3K), whereas control electroporated cells never showed such phenotypes (Figures 3H and 3J). We also noticed that the ectopic GFAP+ *Gli3* mutant cells in the SVZ formed elongated processes similar to the radial processes of NSCs rather than short processes of typical astrocytes (Figure 3I).

Previous studies showed that pSTAT3 directly activates *GFAP* gene transcription by binding to its promoter sequence (Takizawa et al., 2001). Thus, we tested whether the GFAP overexpression seen in $NC;Gli3^{cko}$ mutants was due to the overactivation of STAT3. We treated $NC;Gli3^{cko}$ embryos with a STAT3 inhibitor (WP1066) between E16.5 and birth via pregnant dams and found that GFAP expression at P7 was largely restored to control levels by the STAT3 inhibitor (Figures 3C–3F).

Together, our results indicate that the loss of Gli3R resulted in an increased level of gp130 and its ligands to ectopically induce STAT3-mediated GFAP expression in the $NC;Gli3^{cko}$ mutant SVZ. This eventually made the mutant SVZ cells maintain both NSC and ependymal cell characteristics and fail to develop into two distinct, functional cell types.

Loss of *Gli3* Results in Alterations in Cell Adhesion and Loss of Numb via LNX2

Although the STAT3 inhibitor did rescue the ectopic expression of GFAP, it did not rescue the disruption of the pinwheel arrangement of NSCs and ependymal cells in $NC;Gli3^{cko}$ mutants (Figures 1E and 3F). Thus, we assessed an alternative role for Gli3 in establishing the neurogenic niche structure. We found that in the absence of *Gli3*, the pinwheel organization was not maintained and the ventricular wall integrity was compromised, leading to hydrocephalus. The weakness of the ventricular wall integrity led us to the idea that *Gli3* might regulate cell adhesion between ependymal cells and NSCs. Interestingly, our $NC;Gli3^{cko}$ mutant phenotype is very similar to the reported phenotype of *Numb;Numblike* double-conditional mutants, including reduced cortical thickness and hydrocephaly (Kuo et al., 2006; Wang et al., 2011). Thus, we asked whether Numb levels might have been altered in *Gli3* mutants. We found that levels of Numb protein were greatly reduced in E18.5 $Gli3^{Xt/Xt}$ null mutants (Figure 4A). The SVZ of $NC;Gli3^{cko}$ mutants also showed a reduction in Numb expression at E14.5 and almost complete loss by E18.5, particularly in the outermost cell layer lining the lateral ventricle (Figure 4B).

To explore the mechanism responsible for this loss of Numb, we next examined the expression level of LNX2, an E3 ubiquitin ligase that is known to target Numb for degradation (Nie et al., 2004). We found that the LNX2 protein level was greatly increased in the forebrain extracts of E18.5 $Gli3^{Xt/Xt}$ null embryos compared to the littermate controls (Figure 4C). $NC;Gli3^{cko}$ mutants also showed elevated LNX2 protein levels as assessed by immunohistochemical staining, particularly in the SVZ (Figure 4D). Our findings suggest that the loss of *Gli3* led to an abnormal increase in LNX2 expression that ultimately targeted Numb for degradation in $NC;Gli3^{cko}$ mutants.

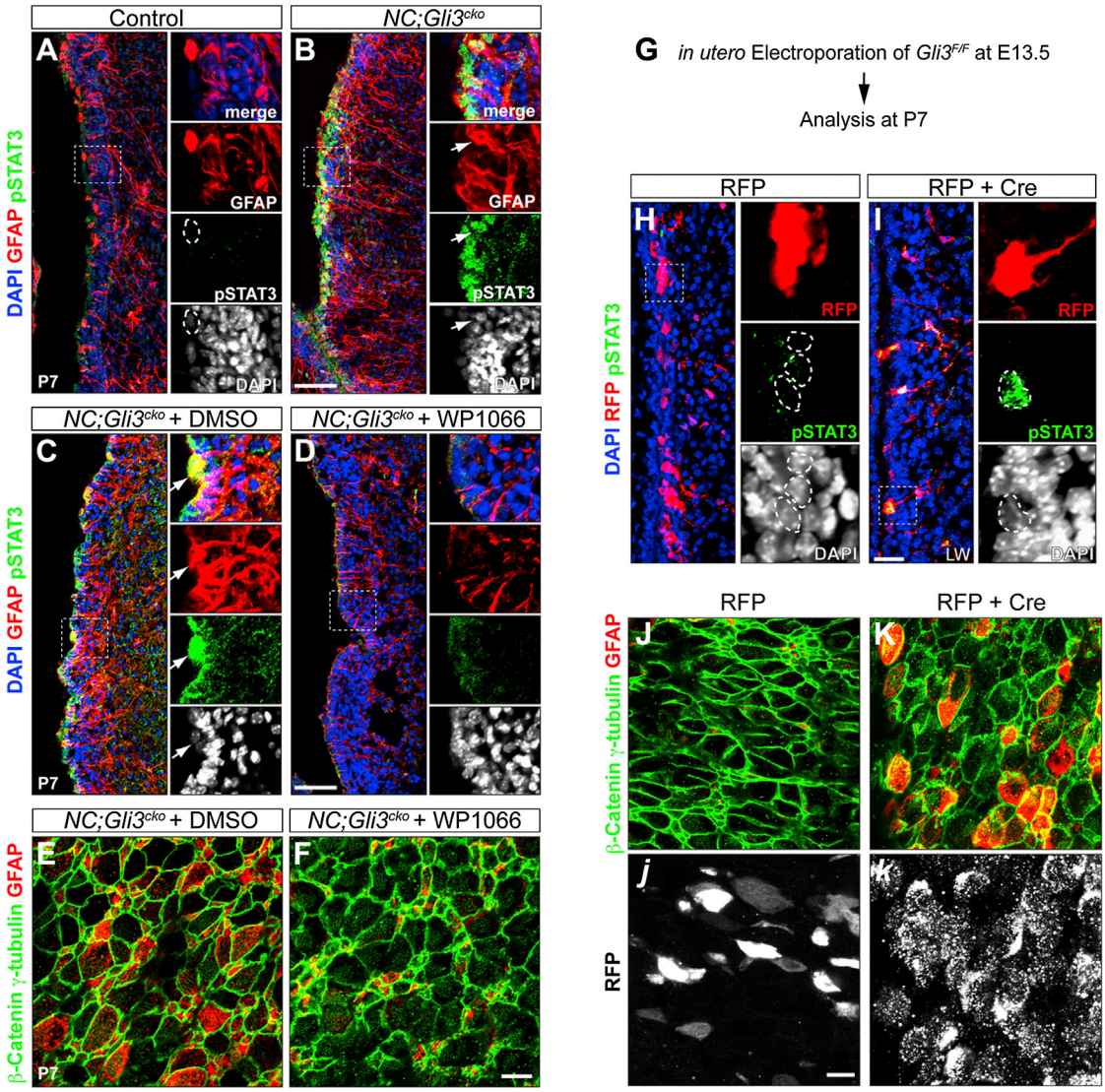

Figure 3. Loss of *Gli3* Leads to the Overactivation of STAT3 and Ectopic GFAP Expression in *NC;Gli3*^{cko} Mutant SVZ

(A and B) Immunohistochemistry of pSTAT3 and GFAP in control and *NC;Gli3*^{cko} SVZ at P7. Both pSTAT3 (green) and GFAP (red) are increased in *NC;Gli3*^{cko} (B) compared to control (A). Higher-magnification images of boxed areas are shown in right panels. GFAP+ cell (outlined by dashed circle) does not express pSTAT3 in the control. Arrows indicate that the GFAP+ cell expresses a high level of nuclear pSTAT3 in the mutant. Scale bar, 50 μm.

(C and D) *NC;Gli3*^{cko} embryos received either STAT3 inhibitor (WP1066) or vehicle control DMSO from E16.5 till birth. The animals were analyzed at P7. The nuclear pSTAT3 (green) in GFAP+ (red) cells shown in mutants receiving DMSO (C) is rescued by WP1066 (D). Arrows indicate that the GFAP+ cell expresses a high level of nuclear pSTAT3 in the DMSO-treated mutant. Scale bar, 50 μm.

(E and F) En face view of P7 *NC;Gli3*^{cko} SVZ that was treated with either STAT3 inhibitor (WP1066) or vehicle control DMSO prenatally. The ectopic GFAP expression (red) in ependymal-like cells (β-catenin+ γ-tubulin+, green) in *NC;Gli3*^{cko} treated with DMSO (E) is rescued by WP1066 (F). Scale bar, 50 μm.

(G–K) In utero electroporation of either RFP alone or RFP + Cre into *Gli3*$^{F/F}$ embryos. Electroporation was done at E13.5, and the manipulated pups were sacrificed at P7. The *Gli3* mutant cells induced by Cre are labeled by RFP in (I). The electroporated cells that received RFP alone (red) do not have nuclear pSTAT3 (green) expression (indicated by dashed circles in H). However, the *Gli3* mutant cells (red) express nuclear pSTAT3 (green) (indicated by dashed circles in I). Scale bar, 25 μm. En face view shows that *Gli3* mutant cells (white in *k*) exhibit ectopic GFAP expression (red in K) in ependymal-like cells (β-catenin+ γ-tubulin+, green). The ectopic GFAP expression is absent in cells that received RFP alone (white in *j*). Scale bar, 50 μm.

See also Figure S3.

Loss of Numb Results in Loss of Proper Cell Adhesion

Because the loss of Numb is associated with defects in cell adhesion (Rasin et al., 2007), we next examined changes in cell adhesion molecules in our *NC;Gli3*^{cko} mutants. In particular, Numb is known to regulate cell adhesion molecules such as E-cadherin, which is critical for proper NSC function and NSC polarity by maintaining adherens junctions (Rasin et al., 2007; Karpowicz et al., 2009; Chenn et al., 1998; Perez-Moreno et al., 2003). When we analyzed changes in E-cadherin expression, we found that the enriched E-cadherin expression seen in

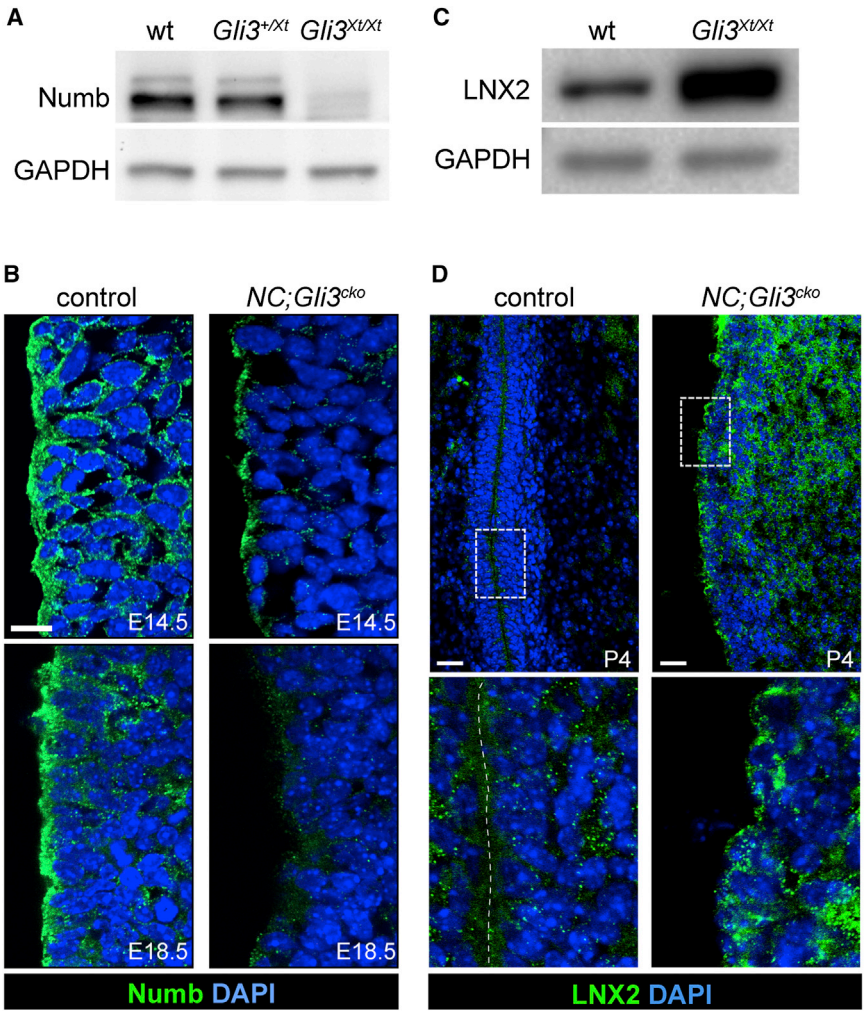

Figure 4. Loss of *Gli3* Results in Decreased Level of Numb Protein

(A) Western blot of Numb in E18.5 $Gli3^{Xt/Xt}$ forebrain shows a dose-dependent reduction in Numb protein level compared to the WT.

(B) Immunohistochemistry of Numb shows that Numb (green) is localized to the ventricular surface of RGCs at both E14.5 and E18.5 in the control (left panels). In $NC;Gli3^{cko}$ mice, Numb is significantly reduced at both E14.5 and E18.5 (right panels). Scale bar, 10 μm.

(C) Western blot of E18.5 forebrain samples shows that LNX2 protein level is increased in $Gli3^{Xt/Xt}$ compared to WT.

(D) Immunohistochemistry of LNX2 at P4 shows that LNX2 (green) protein level is increased at the ventricular surface and in the basal SVZ in $NC;Gli3^{cko}$ mutant (right panels) as compared to the control (left panels). Higher-magnification images of boxed areas are shown below. Scale bars, 10 μm.

the first cell layer of control SVZ was dramatically reduced on the apical surface of the lateral ventricle in $NC;Gli3^{cko}$ mutants at E18.5 (Figures 5A and 5B).

The reduction in E-cadherin expression was also found in the P7 $NC;Gli3^{cko}$ mutant as in the E18.5 analysis. Although there was a clean contiguous E-cadherin expression on the apical surface of the SVZ in controls, there was almost no E-cadherin expression found along the surface of the mutant lateral ventricle (Figures 5C and 5D). Instead, we observed strong E-cadherin expression two to three cell layers below the ventricular surface in the $NC;Gli3^{cko}$ mutants as compared to the controls (Figure 5D, white arrows). Thus, E-cadherin is mislocalized and downregulated during early establishment of the postnatal neurogenic niche.

At P7, we also saw that the well-organized ependymal layer observed in control sections (Figure 5C) was not present in the $NC;Gli3^{cko}$ mutants (Figure 5D). Instead, the first layer of cells failed to form a smooth continuous ventricular surface, and the majority of them expressed GFAP, directly exposing GFAP+ cells to the apical surface of the lateral ventricle (Figure 5D). Interestingly, we found that the cells with the highest E-cadherin expression (black arrow in Figure 5D schematic) in the $NC;Gli3^{cko}$ mutants were also the cells with very low GFAP expression. Our finding that gross disorganization of the ventricular surface observed in the $NC;Gli3^{cko}$ mutants does not occur until postnatal stages (Figures 5B and 5D) further supports the idea that Gli3R is critical during the transition from RGCs to ependymal cells and NSCs, and that cell adhesion is critical for proper neurogenic niche maturation.

To further assess changes in cell adhesion induced by the loss of Gli3R, we examined VCAM1 expression in the SVZ neurogenic niche. VCAM is an adhesion molecule expressed in both NSCs and ependymal cells, although its expression was found to be 8.87 times higher in NSCs than ependymal cells as assessed by quantitative PCR (Figure S4A). VCAM localizes specifically to NSC-ependymal cell junctions (Kokovay et al., 2012), providing a tool for the assessment of cell adhesion and organization of the SVZ. We found that in P21 $NC;Gli3^{cko}$ mutants, VCAM was diffusely expressed throughout the cytoplasm (asterisk in Figure 5f′; Figure S4B), with a pixel intensity five times greater than that of the control (Figures 5e′ and 5H). Furthermore, there was also a significant upregulation of VCAM staining found in the membrane of the mutant cells (open arrowheads in Figures 5F and f′), as opposed to specifically clustering at NSC-ependymal cell junctions (white arrowheads in Figures 5E and 5F). When the number of VCAM+ spots was counted, more than double the amount of membrane-enriched spots was present in the $NC;Gli3^{cko}$ mutants as compared to the controls (Figure 5G). Thus, there is more VCAM present in the cytoplasm and at non-ependymal cell-NSC junctions in the mutants as compared to the control. This ectopic expression suggests that VCAM may not be properly localized within the cell in the absence of *Gli3*,

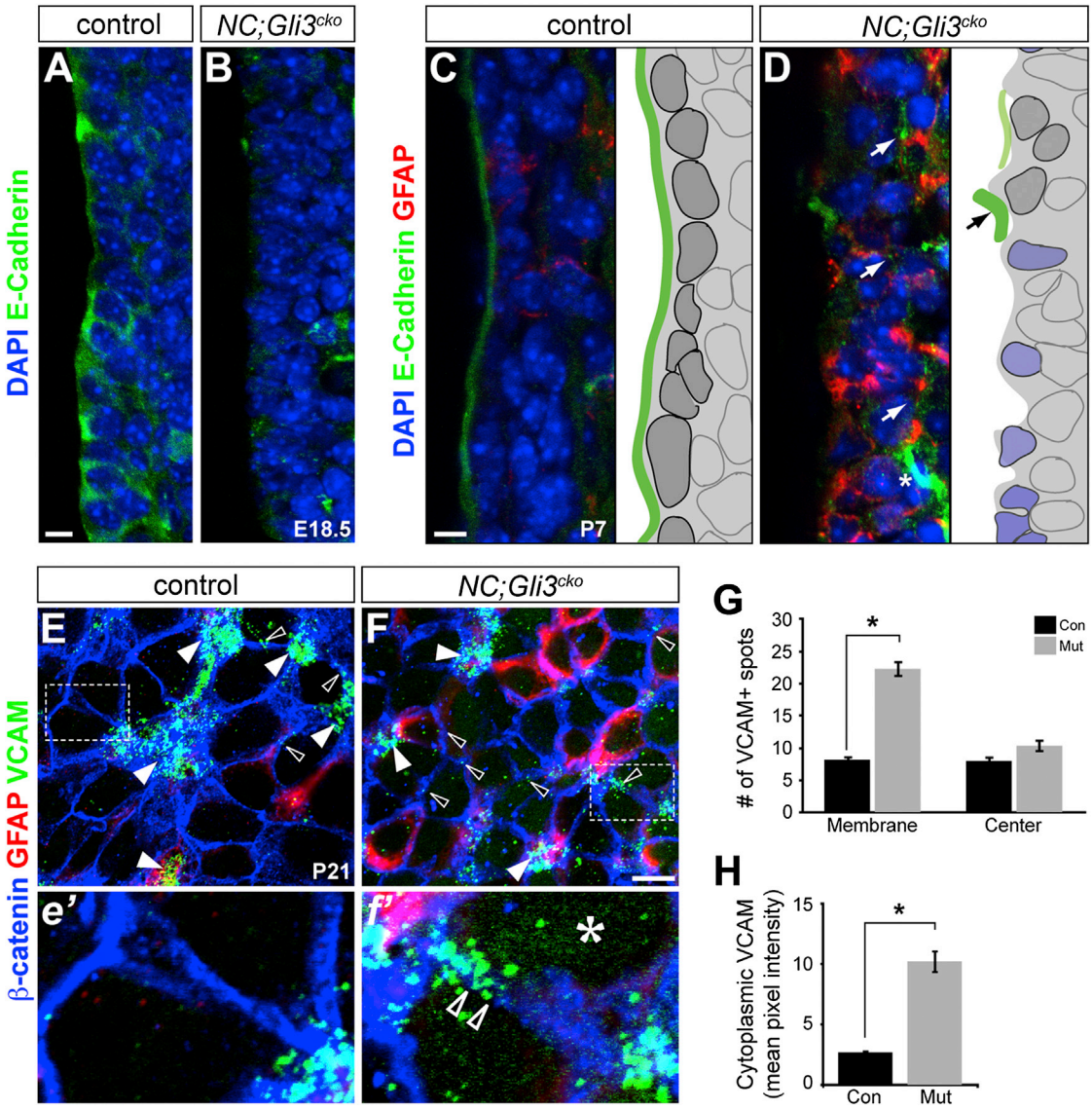

Figure 5. Distribution of Adhesion Molecules Is Disrupted in *NC;Gli3^{cko}*

(A and B) E-Cadherin protein (green) is highly expressed at the apical surface of RGCs in the control mice at E18.5 (A) but is reduced at the apical surface in *NC;Gli3^{cko}* mutants (B). Scale bar, 10 μm.

(C and D) E-Cadherin protein (green) is expressed just at the ventricular surface by ependymal cells at P7 in control mice (C). *NC;Gli3^{cko}* mice show reduced E-Cadherin expression and increased GFAP (red) compared to the control (D). Schematics of immunohistochemical results are shown to the right of each image. Dark-gray cells represent ependymal cells. Blue cells represent atypical mutant cells. Green lines represent E-Cadherin lining. Scale bars, 10 μm. White arrows indicate E-Cadherin expression in the basal SVZ. The black arrow indicates E-Cadherin staining at the apical surface of the SVZ. The star indicates a blood vessel. Scale bars, 10 μm.

(E and F) Whole-mount immunohistochemical staining of the ventricular surface at P21 reveals VCAM1 (green) protein localization in *NC;Gli3^{cko}* (F and *f′*) versus controls (E and *e′*). Higher magnification of inset is shown below low-magnification images (*e′* and *f′*). GFAP (red) marks NSC. Open arrowheads show membrane localization of VCAM that is not associated with NSC clusters. White arrowheads show VCAM staining clustered at pinwheel centers. The asterisk (*f′*) shows the upregulation of VCAM in the cytoplasm of mutant cells. Scale bar, 10 μm (E and F).

(G) Quantification of VCAM spots. A total of 10–15 images for each genotype were counted. Areas of staining above background were considered a VCAM+ spot. If the cluster was at the center of a pinwheel, it was deemed a "cluster" spot, and if at the membrane between two cells a "membrane" spot. All were normalized to spots/image. There were significantly more spots at the membrane of mutant animals as compared to controls. Error bars represent SEM. *$p < 0.05$.

(H) Quantification of cytoplasmic VCAM staining. ImageJ was used to quantify VCAM pixel intensity for each image using a filter based on β-catenin staining to remove VCAM staining localized to the membrane. The mutant images had significantly increased cytoplasmic VCAM as compared to the controls. Error bars represent SEM. *$p < 0.05$.

See also Figure S4.

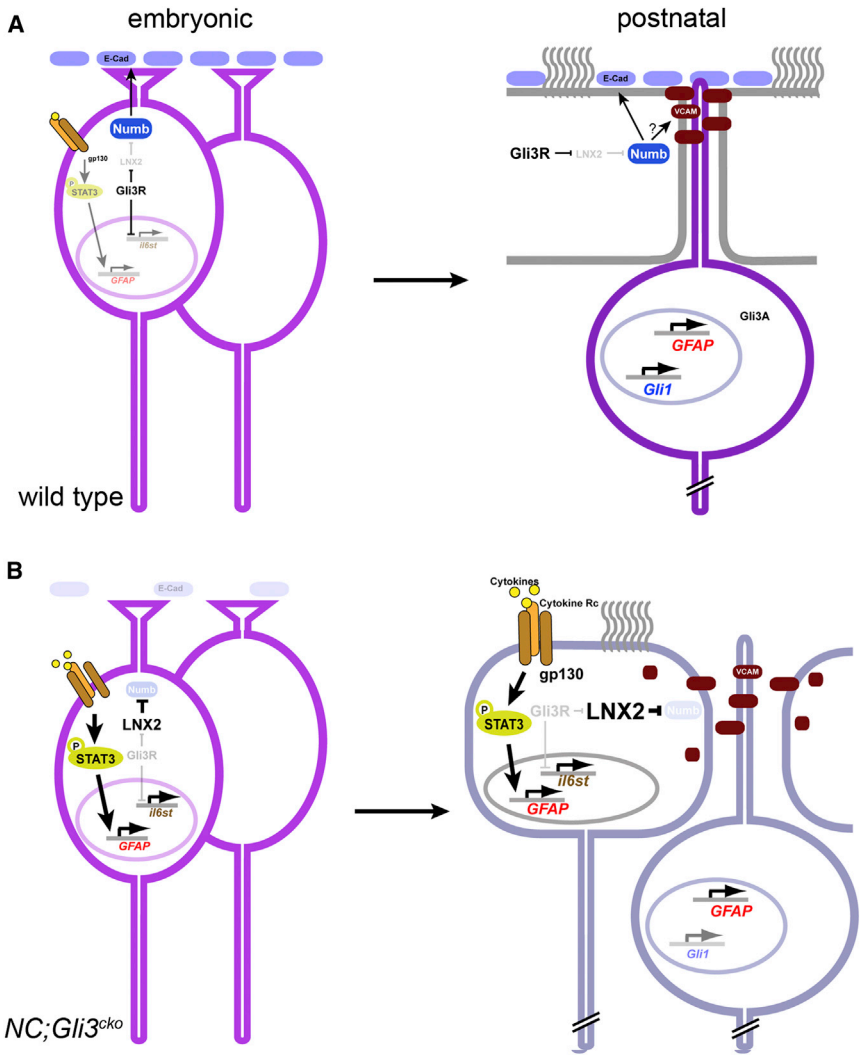

Figure 6. Summary Schematic of Gli3R

(A) In WT animals, embryonic radial glia express Gli3R and suppress *il6st*. Thus, gp130-mediated STAT3 signaling is only transiently activated in future NSCs around birth. Due to Gli3R-mediated suppression of LNX2, the Numb level is maintained to regulate E-cadherin at the apical surface of the VZ. In the postnatal brain, Shh-responding NSCs contain Gli activators to induce GFAP and Gli1 expression, whereas nonresponsive ependymal cells contain Gli3 as Gli3R. Sustained expression of Numb enables ependymal cells to localize E-cadherin and VCAM on the apical surface to maintain the integrity of the neurogenic niche.

(B) In *NC;Gli3*^{cko}, *il6st* is overexpressed due to the loss of Gli3R, resulting in sustained activation of STAT3 to induce GFAP overexpression. Without Gli3R, LNX2 is overexpressed to target Numb for degradation, leading to a loss of E-cadherin on the apical surface of the VZ. In the postnatal brain, cellular characteristics of ependymal cells and NSCs are less distinct, and GFAP is overexpressed across the cell types in the SVZ due to the persistent activation of STAT3. In addition, due to the lack of Numb, E-cadherin is missing from the apical lining of the ventricle, and VCAM is found also in the cytoplasm. Together, these molecular changes lead to the compromised integrity of the neurogenic SVZ structure.

suggesting that there are long-term cell adhesion changes when *Gli3* is lost during development of the SVZ.

DISCUSSION

NSCs and ependymal cells share a common developmental origin (RGCs) in the embryonic LGE and form highly structured arrangements on the ventricular surface of the postnatal SVZ (Kriegstein and Alvarez-Buylla, 2009; Ihrie and Alvarez-Buylla, 2011). Little is known about the manner by which embryonic RGCs transform into NSCs and ependymal cells because most studies have focused on the stages after cell fates are already specified. However, it is clear that there are many changes in signaling between embryonic RGCs and postnatal NSCs. Here, we propose to define three stages of postnatal neurogenic niche development and maturation: first, embryonic RGCs in the LGE; second, transition from embryonic RGCs to postnatal NSCs (~E18.5 to P7); and third, maturation of postnatal NSCs. Our results demonstrate an interesting biphasic requirement of Shh pathway components in these stages for niche maturation. In RGCs, Gli3R is highly expressed, and RGCs are refractory to Shh activation. During the transition between E18.5 and P7, Gli3R plays a critical role in cell fate specification and niche organization, establishing a framework of support cells and stem cells. Finally, once the niche has established (at around P7), Shh-responsive NSCs begin active postnatal neurogenesis. Thus, we have found that Gli3 plays a critical role in setting the stage on which Shh can act in the mature niche.

During the establishment phase of the neurogenic SVZ, several molecular changes take place when *Gli3* is lost (Figure 6). Among several signaling pathways known to influence postnatal neurogenesis in rodent brains, we found that the coordinated activation and duration of Shh and JAK/STAT3 signaling are critical in determination of NSC and ependymal cell fates. Before birth, RGCs do not actively respond to Shh or cytokine signaling. Just around birth, RGCs that gain responsiveness to both Shh and activated STAT3 become NSCs, whereas RGCs remaining unresponsive to these signals become ependymal cells. In addition, unlike Shh signaling that remains active in postnatal NSCs, STAT3 signaling is active only transiently for proper development of the SVZ structure. When STAT3 activation is sustained due to the overexpression of *il6st* (gp130) in *NC;Gli3*^{cko} mutants, ectopic GFAP expression is widespread across the cell types, resulting in compromised cell fates in the SVZ niche. Thus, whereas transient STAT3 signaling is necessary for NSC specification, sustained STAT3 signaling is detrimental to the proper

specification of cell types generated from RGCs during the establishment period of the neurogenic niche. A recent study reported that adult NSCs in the SVZ express CNTF receptors and respond to exogenous CNTF in vivo (Lee et al., 2013). Because CNTF signaling promotes self-renewal of the SVZ NSCs in vitro (Shimazaki et al., 2001; Müller et al., 2009), the fact that NSCs still retain CNTF receptor expression may indicate their potential to respond to exogenously supplied cytokines. Interestingly, the cytokines of IL-6 family are commonly induced by inflammation, suggesting that diseases or injuries in the SVZ might induce changes in NSC behavior through activated STAT3 signaling.

In addition to its role in the regulation of Shh and STAT3 signaling, our current findings demonstrate a key role for Gli3R in the establishment of the neurogenic niche structure through the maintenance of Numb (Figure 6). Interestingly, we found that in WT animals, *Numb* mRNA is expressed at a higher level in ependymal cells than in their neighboring NSCs (Figure S1C). Because Numb is a negative regulator of Notch signaling, our result supports the previously reported phenomenon that positive Notch activity is only observed in NSCs, not in ependymal cells (Imayoshi et al., 2010). However, the absence of Numb did not affect Notch activity in *NC;Gli3*^{cko} mutants as evidenced by lack of significant change in *Hes5* expression, a readout of activated Notch signaling (data not shown). Thus, Numb is not affecting the SVZ structure through alteration of Notch activity as expected. Because Numb is also known to suppress Shh signaling via targeted degradation of Gli1 (Pierfelice et al., 2011; Di Marcotullio et al., 2006), the absence of Numb in *NC;Gli3*^{cko} mutants could be responsible for a slight induction of Shh response observed in mutant ependymal cells (Figures S1H and S1I), which may contribute to the less-distinct cell identities.

Although loss of Numb does appear to affect Shh signaling, the primary consequence of its loss in our *NC;Gli3*^{cko} mutants was the disorganization of the niche structure due to defects in cell adhesion (Kuo et al., 2006). We showed that a loss of Numb in our *NC;Gli3*^{cko} mutants resulted in changes in adherens junctions between niche cells as evidenced by altered VCAM and E-cadherin expression and localization. Because Numb-mediated loss of E-cadherin is known to change gap junctions between cells (Govindarajan et al., 2010), similar defects in *NC;Gli3*^{cko} mutants could disrupt the communication between NSCs and ependymal cells for extracellular signaling molecules. One consistent and interesting phenotype we observed from acute deletion of *Gli3* using in utero electroporation was that the cellular boundaries of *Gli3* mutant cells expressing the reporter protein RFP (red fluorescent protein) always appeared to be less clear, raising the possibility that electroporated DNA constructs could be more leaky between mutant cells (Figure 3*k*). In addition, entanglement of the GFAP+ processes on the apical surface of the SVZ suggests possible defects in polarity, a role in which Numb was implicated previously in RGCs (Rasin et al., 2007). For example, apical processes of NSCs that are critical for sensing signaling molecules in the CSF of the lateral ventricle (Kokovay et al., 2010; Lehtinen et al., 2011) require proper cell-cell adhesion for their maintenance (Loulier et al., 2009). Thus, structural defects in the SVZ can lead to neurogenic defects when polarity or cell adhesion alterations prevent NSCs from effectively communicating with neighboring cells and factors present in the ventricular lumen/CSF.

Interestingly, we found that there were a few cells in the *NC;Gli3*^{cko} mutants that still expressed normal levels of E-cadherin at P7, when the stereotypical adult neurogenic niche structure emerges (Figure 5D). These cells did not overexpress GFAP and exhibited normal characteristics of true differentiated ependymal cells, suggesting that they were most likely the ones that escaped *NC*-mediated recombination of the *Gli3*^{F} conditional allele and were able to maintain normal Gli3R levels. Thus, the expression of E-cadherin appears to be a fundamental feature of proper ependymal cells, and Gli3R is required for its expression via maintenance of Numb.

In summary, we have identified a role for Gli3R as a critical mediator of cell fate specification and cytoarchitectural organization in the neurogenic niche during the niche establishment phase. We found that Gli3R suppresses glial fates through transcriptional regulation of gp130 and promotes the stable expression and localization of cell adhesion molecules for proper formation of the neurogenic niche cytoarchitecture. Together, our findings provide an interesting biphasic requirement of Shh signaling components in the SVZ neurogenesis: Gli3R shapes the neurogenic niche structure prior to Shh activation, which in turn promotes the neurogenesis. Thus, we have found a crucial role for Gli3R in establishment of the adult neurogenic niche.

EXPERIMENTAL PROCEDURES

Mice and DNA

All procedures in mice followed the guidelines of the Institutional Animal Care and Use Committee of the NIH. *Gli3* conditional (*Gli3*$^{F/+}$) and null (*Gli3*$^{Xt/+}$) alleles as well as *NC* mouse line were previously described by Blaess et al. (2008), Hui and Joyner (1993), and Tronche et al. (1999). In utero electroporation was performed on E13.5 embryos following the procedures described in Wang et al. (2011). More detailed information is listed in Supplemental Experimental Procedures.

Histology, Immunohistochemistry, RNA In Situ Hybridization, and TEM

Brains were dissected from perfused animals, and either frozen sections or vibratome sections were used. Whole-mount analysis of the SVZ structure followed the procedure described in Mirzadeh et al. (2008, 2010). Antibodies used are listed in Supplemental Experimental Procedures. RNA in situ hybridization followed the procedure described in Ahn and Joyner (2004). Tissue processing for TEM and X-gal/TEM was done as described by Wichterle et al. (1999), and cell types were identified according to Doetsch et al. (1997).

Western Analysis and Quantitative Real-Time PCR

Western analysis was performed as described (Ahn and Joyner, 2004). Quantitative real-time PCR was performed on total RNA obtained from embryonic forebrain tissue or fluorescence-activated cell sorting (FACS)-isolated NSCs and ependymal cells from adult mice as detailed in Supplemental Experimental Procedures.

EMSA

Oligonucleotide probes were designed based on the Gli binding site located from −215 to −200 bp 5′ of the mouse *il6st* gene identified by the Evolutionary Conservation of Genomes browser (Ovcharenko et al., 2004). WT probe sequence is 5′-TCCGTTCCGGCCACCCACCCAAGTGCGGCGG-3′. Mutant probe sequence is 5′-TCCGTTCCGGCCATTTATTTAAGTGCGG CGG-3′. Double-stranded oligonucleotides were labeled with digoxigenin-2′,3′-dideoxyuridine-5′-triphosphate using DIG Gel Shift Kit (Roche). Gli3R containing nuclear extract was isolated from pGli3R-IRES-nGFP transfected

293T cells and was used for oligonucleotide binding directly. The binding reaction was set up following previous studies by Vortkamp et al. (1995). A 4%–20% gradient precast Tris-borate-EDTA (TBE) gel (Bio-Rad) was prerun for 30 min, and the electrophoresis was carried out for 90 min at 80 V in 0.5× TBE. Samples were then electrotransferred onto positively charged nylon membrane and subjected to antibody reaction and chemiluminescent detection following the DIG Gel Shift Kit protocol.

STAT3 Inhibitor Treatment

Timed pregnant females carrying *NC;Gli3*^{cko} mutant embryos were given 600 μg/day of either a STAT3 inhibitor, WP1066 (dissolved in DMSO), or DMSO of the same volume starting from E16.5 until birth. Pups were sacrificed at P7 and subjected to section or whole-mount immunohistochemistry.

Quantification and Statistics

Statistical analysis of quantitative real-time PCR and western blotting was performed by Student's t test. The quantification results are presented as average ± SEM for error bars. n indicates the number of animals analyzed. Quantification of cytoplasmic pixel intensity for VCAM expression was performed using ImageJ. A filter was laid over each image using the threshold tool based on membrane staining by β-catenin. Erode and Dilate were used to fill the cytoplasmic area so that the filter was as accurate as possible, then pixel intensity was measured using Analyze Particles. Pixel intensity measurements were collected in Excel, and ANOVA was used to quantify differences between groups. Significance was set at $p < 0.05$.

SUPPLEMENTAL INFORMATION

Supplemental Information includes Supplemental Experimental Procedures and four figures and can be found with this article online at http://dx.doi.org/10.1016/j.celrep.2014.07.006.

AUTHOR CONTRIBUTIONS

H.W., A.W.K., and S.A. designed experiments, analyzed data, and wrote the paper. H.W. performed experiments to characterize the *Gli3* mutant phenotype and to establish the link between gp130 and Gli3. A.K. performed experiments on the Gli3 and Numb relationship via LNX2 and also on cell adhesion phenotype in *Gli3* mutants. C.L. performed cell-type-specific gene expression analysis.

ACKNOWLEDGMENTS

We would like to thank M. Song, M. Zervas, and J. Li for critical reading of the manuscript; I. Dawid and M. Won for helpful suggestions on the LNX2 study; M. Song for discussions on STAT3; members of the S.A. lab for discussion; and G. Ge and E. Karey for help during the initial stage of the study. We would also like to thank NICHD Microscopy Imaging Core and NCI Electron Microscopy Core Facilities for confocal microscopy and TEM analysis; and NHLBI Flow Cytometry Core Facility for FACS. This study was supported by the Intramural Research Program of NIH (1ZIHD008781 to S.A.).

Received: November 1, 2013
Revised: June 13, 2014
Accepted: July 3, 2014
Published: August 7, 2014

REFERENCES

Ahn, S., and Joyner, A.L. (2004). Dynamic changes in the response of cells to positive hedgehog signaling during mouse limb patterning. Cell *118*, 505–516.

Ahn, S., and Joyner, A.L. (2005). In vivo analysis of quiescent adult neural stem cells responding to Sonic hedgehog. Nature *437*, 894–897.

Bai, C.B., Auerbach, W., Lee, J.S., Stephen, D., and Joyner, A.L. (2002). Gli2, but not Gli1, is required for initial Shh signaling and ectopic activation of the Shh pathway. Development *129*, 4753–4761.

Blaess, S., Stephen, D., and Joyner, A.L. (2008). Gli3 coordinates three-dimensional patterning and growth of the tectum and cerebellum by integrating Shh and Fgf8 signaling. Development *135*, 2093–2103.

Bonni, A., Sun, Y., Nadal-Vicens, M., Bhatt, A., Frank, D.A., Rozovsky, I., Stahl, N., Yancopoulos, G.D., and Greenberg, M.E. (1997). Regulation of gliogenesis in the central nervous system by the JAK-STAT signaling pathway. Science *278*, 477–483.

Chenn, A., Zhang, Y.A., Chang, B.T., and McConnell, S.K. (1998). Intrinsic polarity of mammalian neuroepithelial cells. Mol. Cell. Neurosci. *11*, 183–193.

Corrales, J.D., Blaess, S., Mahoney, E.M., and Joyner, A.L. (2006). The level of sonic hedgehog signaling regulates the complexity of cerebellar foliation. Development *133*, 1811–1821.

Di Marcotullio, L., Ferretti, E., Greco, A., De Smaele, E., Po, A., Sico, M.A., Alimandi, M., Giannini, G., Maroder, M., Screpanti, I., and Gulino, A. (2006). Numb is a suppressor of Hedgehog signalling and targets Gli1 for Itch-dependent ubiquitination. Nat. Cell Biol. *8*, 1415–1423.

Di Marcotullio, L., Greco, A., Mazzà, D., Canettieri, G., Pietrosanti, L., Infante, P., Coni, S., Moretti, M., De Smaele, E., Ferretti, E., et al. (2011). Numb activates the E3 ligase Itch to control Gli1 function through a novel degradation signal. Oncogene *30*, 65–76.

Doetsch, F., García-Verdugo, J.M., and Alvarez-Buylla, A. (1997). Cellular composition and three-dimensional organization of the subventricular germinal zone in the adult mammalian brain. J. Neurosci. *17*, 5046–5061.

Fotaki, V., Yu, T., Zaki, P.A., Mason, J.O., and Price, D.J. (2006). Abnormal positioning of diencephalic cell types in neocortical tissue in the dorsal telencephalon of mice lacking functional Gli3. J. Neurosci. *26*, 9282–9292.

Govindarajan, R., Chakraborty, S., Johnson, K.E., Falk, M.M., Wheelock, M.J., Johnson, K.R., and Mehta, P.P. (2010). Assembly of connexin43 into gap junctions is regulated differentially by E-cadherin and N-cadherin in rat liver epithelial cells. Mol. Biol. Cell *21*, 4089–4107.

Herrmann, J.E., Imura, T., Song, B., Qi, J., Ao, Y., Nguyen, T.K., Korsak, R.A., Takeda, K., Akira, S., and Sofroniew, M.V. (2008). STAT3 is a critical regulator of astrogliosis and scar formation after spinal cord injury. J. Neurosci. *28*, 7231–7243.

Hui, C.C., and Joyner, A.L. (1993). A mouse model of greig cephalopolysyndactyly syndrome: the extra-toesJ mutation contains an intragenic deletion of the Gli3 gene. Nat. Genet. *3*, 241–246.

Ihrie, R.A., and Alvarez-Buylla, A. (2011). Lake-front property: a unique germinal niche by the lateral ventricles of the adult brain. Neuron *70*, 674–686.

Imayoshi, I., Sakamoto, M., Yamaguchi, M., Mori, K., and Kageyama, R. (2010). Essential roles of Notch signaling in maintenance of neural stem cells in developing and adult brains. J. Neurosci. *30*, 3489–3498.

Jacquet, B.V., Salinas-Mondragon, R., Liang, H., Therit, B., Buie, J.D., Dykstra, M., Campbell, K., Ostrowski, L.E., Brody, S.L., and Ghashghaei, H.T. (2009). FoxJ1-dependent gene expression is required for differentiation of radial glia into ependymal cells and a subset of astrocytes in the postnatal brain. Development *136*, 4021–4031.

Karpowicz, P., Willaime-Morawek, S., Balenci, L., DeVeale, B., Inoue, T., and van der Kooy, D. (2009). E-Cadherin regulates neural stem cell self-renewal. J. Neurosci. *29*, 3885–3896.

Kokovay, E., Goderie, S., Wang, Y., Lotz, S., Lin, G., Sun, Y., Roysam, B., Shen, Q., and Temple, S. (2010). Adult SVZ lineage cells home to and leave the vascular niche via differential responses to SDF1/CXCR4 signaling. Cell Stem Cell *7*, 163–173.

Kokovay, E., Wang, Y., Kusek, G., Wurster, R., Lederman, P., Lowry, N., Shen, Q., and Temple, S. (2012). VCAM1 is essential to maintain the structure of the SVZ niche and acts as an environmental sensor to regulate SVZ lineage progression. Cell Stem Cell *11*, 220–230.

Kriegstein, A., and Alvarez-Buylla, A. (2009). The glial nature of embryonic and adult neural stem cells. Annu. Rev. Neurosci. *32*, 149–184.

Kuo, C.T., Mirzadeh, Z., Soriano-Navarro, M., Rasin, M., Wang, D., Shen, J., Sestan, N., Garcia-Verdugo, J., Alvarez-Buylla, A., Jan, L.Y., and Jan, Y.N.

(2006). Postnatal deletion of Numb/Numblike reveals repair and remodeling capacity in the subventricular neurogenic niche. Cell *127*, 1253–1264.

Lee, C., Hu, J., Ralls, S., Kitamura, T., Loh, Y.P., Yang, Y., Mukouyama, Y.S., and Ahn, S. (2012). The molecular profiles of neural stem cell niche in the adult subventricular zone. PLoS One *7*, e50501.

Lee, N., Batt, M.K., Cronier, B.A., Jackson, M.C., Bruno Garza, J.L., Trinh, D.S., Mason, C.O., Spearry, R.P., Bhattacharya, S., Robitz, R., et al. (2013). Ciliary neurotrophic factor receptor regulation of adult forebrain neurogenesis. J. Neurosci. *33*, 1241–1258.

Lehtinen, M.K., Zappaterra, M.W., Chen, X., Yang, Y.J., Hill, A.D., Lun, M., Maynard, T., Gonzalez, D., Kim, S., Ye, P., et al. (2011). The cerebrospinal fluid provides a proliferative niche for neural progenitor cells. Neuron *69*, 893–905.

Loots, G.G., and Ovcharenko, I. (2004). rVISTA 2.0: evolutionary analysis of transcription factor binding sites. Nucleic Acids Res. *32*, W217–W221.

Loulier, K., Lathia, J.D., Marthiens, V., Relucio, J., Mughal, M.R., Tang, S.C., Coksaygan, T., Hall, P.E., Chigurupati, S., Patton, B., et al. (2009). beta1 integrin maintains integrity of the embryonic neocortical stem cell niche. PLoS Biol. *7*, e1000176.

Machold, R., Hayashi, S., Rutlin, M., Muzumdar, M.D., Nery, S., Corbin, J.G., Gritli-Linde, A., Dellovade, T., Porter, J.A., Rubin, L.L., et al. (2003). Sonic hedgehog is required for progenitor cell maintenance in telencephalic stem cell niches. Neuron *39*, 937–950.

Mirzadeh, Z., Merkle, F.T., Soriano-Navarro, M., Garcia-Verdugo, J.M., and Alvarez-Buylla, A. (2008). Neural stem cells confer unique pinwheel architecture to the ventricular surface in neurogenic regions of the adult brain. Cell Stem Cell *3*, 265–278.

Mirzadeh, Z., Han, Y.G., Soriano-Navarro, M., García-Verdugo, J.M., and Alvarez-Buylla, A. (2010). Cilia organize ependymal planar polarity. J. Neurosci. *30*, 2600–2610.

Müller, S., Chakrapani, B.P., Schwegler, H., Hofmann, H.D., and Kirsch, M. (2009). Neurogenesis in the dentate gyrus depends on ciliary neurotrophic factor and signal transducer and activator of transcription 3 signaling. Stem Cells *27*, 431–441.

Nakashima, K., and Taga, T. (2002). Mechanisms underlying cytokine-mediated cell-fate regulation in the nervous system. Mol. Neurobiol. *25*, 233–244.

Nakashima, K., Wiese, S., Yanagisawa, M., Arakawa, H., Kimura, N., Hisatsune, T., Yoshida, K., Kishimoto, T., Sendtner, M., and Taga, T. (1999a). Developmental requirement of gp130 signaling in neuronal survival and astrocyte differentiation. J. Neurosci. *19*, 5429–5434.

Nakashima, K., Yanagisawa, M., Arakawa, H., Kimura, N., Hisatsune, T., Kawabata, M., Miyazono, K., and Taga, T. (1999b). Synergistic signaling in fetal brain by STAT3-Smad1 complex bridged by p300. Science *284*, 479–482.

Nie, J., Li, S.S., and McGlade, C.J. (2004). A novel PTB-PDZ domain interaction mediates isoform-specific ubiquitylation of mammalian Numb. J. Biol. Chem. *279*, 20807–20815.

Ovcharenko, I., Nobrega, M.A., Loots, G.G., and Stubbs, L. (2004). ECR Browser: a tool for visualizing and accessing data from comparisons of multiple vertebrate genomes. Nucleic Acids Res. *32*, W280–W286.

Paez-Gonzalez, P., Abdi, K., Luciano, D., Liu, Y., Soriano-Navarro, M., Rawlins, E., Bennett, V., Garcia-Verdugo, J.M., and Kuo, C.T. (2011). Ank3-dependent SVZ niche assembly is required for the continued production of new neurons. Neuron *71*, 61–75.

Perez-Moreno, M., Jamora, C., and Fuchs, E. (2003). Sticky business: orchestrating cellular signals at adherens junctions. Cell *112*, 535–548.

Pierfelice, T., Alberi, L., and Gaiano, N. (2011). Notch in the vertebrate nervous system: an old dog with new tricks. Neuron *69*, 840–855.

Rasin, M.R., Gazula, V.R., Breunig, J.J., Kwan, K.Y., Johnson, M.B., Liu-Chen, S., Li, H.S., Jan, L.Y., Jan, Y.N., Rakic, P., and Sestan, N. (2007). Numb and Numbl are required for maintenance of cadherin-based adhesion and polarity of neural progenitors. Nat. Neurosci. *10*, 819–827.

Schimmang, T., Lemaistre, M., Vortkamp, A., and Rüther, U. (1992). Expression of the zinc finger gene Gli3 is affected in the morphogenetic mouse mutant extra-toes (Xt). Development *116*, 799–804.

Shen, Q., Wang, Y., Kokovay, E., Lin, G., Chuang, S.-M., Goderie, S.K., Roysam, B., and Temple, S. (2008). Adult SVZ stem cells lie in a vascular niche: a quantitative analysis of niche cell-cell interactions. Cell Stem Cell *3*, 289–300.

Shimazaki, T., Shingo, T., and Weiss, S. (2001). The ciliary neurotrophic factor/leukemia inhibitory factor/gp130 receptor complex operates in the maintenance of mammalian forebrain neural stem cells. J. Neurosci. *21*, 7642–7653.

Spassky, N., Merkle, F.T., Flames, N., Tramontin, A.D., García-Verdugo, J.M., and Alvarez-Buylla, A. (2005). Adult ependymal cells are postmitotic and are derived from radial glial cells during embryogenesis. J. Neurosci. *25*, 10–18.

Takizawa, T., Nakashima, K., Namihira, M., Ochiai, W., Uemura, A., Yanagisawa, M., Fujita, N., Nakao, M., and Taga, T. (2001). DNA methylation is a critical cell-intrinsic determinant of astrocyte differentiation in the fetal brain. Dev. Cell *1*, 749–758.

Tavazoie, M., Van der Veken, L., Silva-Vargas, V., Louissaint, M., Colonna, L., Zaidi, B., Garcia-Verdugo, J.M., and Doetsch, F. (2008). A specialized vascular niche for adult neural stem cells. Cell Stem Cell *3*, 279–288.

Theil, T., Alvarez-Bolado, G., Walter, A., and Rüther, U. (1999). *Gli3* is required for *Emx* gene expression during dorsal telencephalon development. Development *126*, 3561–3571.

Tronche, F., Kellendonk, C., Kretz, O., Gass, P., Anlag, K., Orban, P.C., Bock, R., Klein, R., and Schütz, G. (1999). Disruption of the glucocorticoid receptor gene in the nervous system results in reduced anxiety. Nat. Genet. *23*, 99–103.

Vokes, S.A., Ji, H., Wong, W.H., and McMahon, A.P. (2008). A genome-scale analysis of the cis-regulatory circuitry underlying sonic hedgehog-mediated patterning of the mammalian limb. Genes Dev. *22*, 2651–2663.

Vortkamp, A., Gessler, M., and Grzeschik, K.H. (1995). Identification of optimized target sequences for the GLI3 zinc finger protein. DNA Cell Biol. *14*, 629–634.

Wang, H., Ge, G., Uchida, Y., Luu, B., and Ahn, S. (2011). Gli3 is required for maintenance and fate specification of cortical progenitors. J. Neurosci. *31*, 6440–6448.

Wichterle, H., Garcia-Verdugo, J.M., Herrera, D.G., and Alvarez-Buylla, A. (1999). Young neurons from medial ganglionic eminence disperse in adult and embryonic brain. Nat. Neurosci. *2*, 461–466.

Young, K.M., Fogarty, M., Kessaris, N., and Richardson, W.D. (2007). Subventricular zone stem cells are heterogeneous with respect to their embryonic origins and neurogenic fates in the adult olfactory bulb. J. Neurosci. *27*, 8286–8296.

Zhou, P., Alfaro, J., Chang, E.H., Zhao, X., Porcionatto, M., and Segal, R.A. (2011). Numb links extracellular cues to intracellular polarity machinery to promote chemotaxis. Dev. Cell *20*, 610–622.